Journal of Materials Chemistry A

Identifying Structure-Function Relationships to Modulate Crossover in Nonaqueous Redox Flow Batteries

Journal:	*Journal of Materials Chemistry A*
Manuscript ID	TA-ART-05-2023-002633.R1
Article Type:	Paper
Date Submitted by the Author:	17-Aug-2023
Complete List of Authors:	Jett, Brianna; University of Michigan, Department of Chemistry Flynn, Autumn; University of Utah, Department of Chemistry Sigman, Matthew ; University of Utah, Department of Chemistry Sanford, Melanie; University of Michigan, Department of Chemistry

ARTICLE

Identifying Structure-Function Relationships to Modulate Crossover in Nonaqueous Redox Flow Batteries

Received 00th January 20xx,
Accepted 00th January 20xx

DOI: 10.1039/x0xx00000x

Brianna Jett,[a,c,d] Autumn Flynn,[b,c,d] Matthew S. Sigman ,*[,b,d] and Melanie S. Sanford*[,a,d]

Nonaqueous redox flow batteries (NARFBs) offer a promising solution for large-scale storage of renewable energy. However, crossover of redox active molecules between the two sides of the cell is a major factor limiting their development, as most selective separators are designed for deployment in water, rather than organic solvents. This report describes a systematic investigation of the crossover rates of redox active organic molecules through an anion exchange separator under RFB-relevant non-aqueous conditions (in acetontrile/KPF_6) using a combination of experimental and computational methods. A structurally diverse set of neutral and cationic molecules was selected, and their rates of crossover were determined experimentally with the organic solvent-compatible anion exchange separator Fumasep FAP-375-PP. The resulting data were then fit to various descriptors of molecular size, charge, and hydrophobicity (overall charge, solution diffusion coefficient, globularity, dynamic volume, dynamic surface area, clogP). This analysis resulted in multiple statistical models of crossover rates for this separator. These models were then used to predict tether groups that dramatically slow the crossover of small organic molecules in this system.

Introduction

Redox flow batteries (RFBs) are a promising energy storage technology for integrating renewable energy sources into the electrical grid.[1-3] Most commercial RFBs use aqueous solutions of transition metal salts as the energy storage materials.[4,5] However, recent efforts have focused on redox-active organic molecules (ROMs) as cost effective, sustainable, and tunable alternatives.[6-13] In these systems, energy generated from renewable sources is stored as chemical charge in a pair of organic molecules—an anolyte (which is reduced during battery charging) and catholyte (which is oxidized during battery charging).[9,14] ROMs are particularly well suited for applications in non-aqueous solvents, whose wide potential windows enable larger cell potentials than are commonly accessible in water.[8,15] The optimal non-aqueous RFB has an asymmetric configuration, with the catholyte isolated on one side of the electrochemical cell and the anolyte on the other. These two half-cells are connected by a separator, which must enable rapid diffusion of charge-balancing supporting ions while impeding crossover of the redox-active molecules.[16-18]

Over the past decade, there has been considerable progress in the discovery of ROMs that possess the molecular properties required for non-aqueous RFBs, including high (catholyte) and low (anolyte) redox potentials as well as high solubility and stability to redox cycling.[19-23] However, crossover of the anolyte and catholyte between the two battery half cells remains a major challenge in non-aqueous media. Currently, the most effective approach for separating organic anolytes and catholytes in non-aqueous RFBs is based on size exclusion.[24-27] For instance, mesoporous separators such as Celgard or Daramic have been combined with polymer-supported ROMs.[25,26,28] Here, the large size of the polymer slows diffusion through the separator. In a related approach, microporous separators have been combined with oligomeric ROMs.[24,29,30] Again, separation is achieved through size exclusion based on the relative size of the pores compared to that of the oligomers. However, despite these successes, oligomeric/polymeric systems can be limited by slow rates of diffusion, high viscosities, and low current densities.[24-30]

More recently our groups[17,19,22,31,32] and others[33-35] have begun to explore anion exchange membranes (AEMs) to separate non-aqueous RFBs. However, this remains challenging because most commercial AEMs are designed for applications in water (e.g., desalination, bioreactors, fuel cells, aqueous RFBs).[36-39] As such, these materials are highly effective at separating aqueous solutions of cations based on Coulombic repulsion (with tri-cation > di-cation > mono-cation >> neutral).[40] In contrast, many AEMs are incompatible with non-aqueous solvents, which lead to swelling and/or dissolution of the separator.[33,37] Additionally, the Coulombic repulsion between a cationic solute and an AEM is dramatically impacted by the different solvation of ions in organic media (which typically involves much less solvent separation than in water).[15,41-43] Overall, despite interest in identifying AEMs that

[a] Department of Chemistry, University of Michigan, 930 N University Ave, Ann Arbor, MI 48109, United States
[b] Department of Chemistry, University of Utah, 315 South 1400 East, Salt Lake City, Utah 84112, United States
[c] These authors contributed equally.
[d] Joint Center for Energy Storage Research, 9700 S. Cass Avenue, Argonne, Illinois 60439, United States
Electronic Supplementary Information (ESI) available: [details of any supplementary information available should be included here]. See DOI: 10.1039/x0xx00000x

effectively and predictably separate ROM solutions in non-aqueous RFBs, existing studies remain largely empirical. This gap motivates systematic modelling of how the molecular properties of ROMs impact crossover in organic media.

In this study, we seek to disentangle the contributions of ROM molecular structure to crossover rates in acetonitrile (MeCN) with the commercial AEM Fumasep FAP-375-PP.[44,45] Experimental crossover rates for a training set of structurally diverse ROMs are analyzed by multivariate linear regression (MLR) with various chemical descriptors. Moderate correlation is observed with the overall charge of the molecule, but there is significant variation within a given charge state (0, +1, +2). To effectively model and explain this variation, we develop several statistical models that correlate crossover rate to computed molecular properties, by incorporating descriptors such as globularity, dynamic volume, dynamic surface area, and clogP. Furthermore, we show that this approach effectively predicts tether groups that can be appended to slow crossover of monomeric ROMs by close to a factor of 50. We anticipate that this approach will prove broadly useful for designing and characterizing new separators, catholytes, and anolytes for non-aqueous RFBs.

Dataset

From a set of 73, we selected 20 structurally and electronically diverse redox active small molecules as a training set for constructing statistical models (Figure 1A). These 20 compounds were selected by calculating low-level Mordred descriptors of the available ROMs (ROM pool detailed in the SI), and then using K-means clustering and the elbow method to determine the ideal number of representative clusters and to identify their centroids.[46-48] The AEM Fumasep FAP-375-PP was selected as the separator based on its prior implementation in nonaqueous RFBs with MeCN/KPF_6 as the supporting electrolyte.[19,20,22,49] This is a rare example of a commercial AEM that has been shown to be compatible with non-aqueous RFBs.

The rate of crossover was determined experimentally for each ROM in a Fumasep FAP-375-PP-separated H-cell by loading a 25 mM solution of ROM in MeCN/KPF_6 into the retentate side of the cell and monitoring the permeate by cyclic voltammetry as a function of time. The initial first order rate was then measured from plots of concentration versus time over the first 10% of crossover (Figure 1B).[50] As summarized in Figure 1C, the initial rates varied over two orders of magnitude, from 2.95 to 0.03 mM/h.[51] In general, the neutral ROMs (**1-10**) show relatively fast initial rates of crossover that span from 0.55 (**7**) to 2.95 (**1**) mM/h. The trication **20** exhibits the slowest rate of crossover (0.03 mM/h).

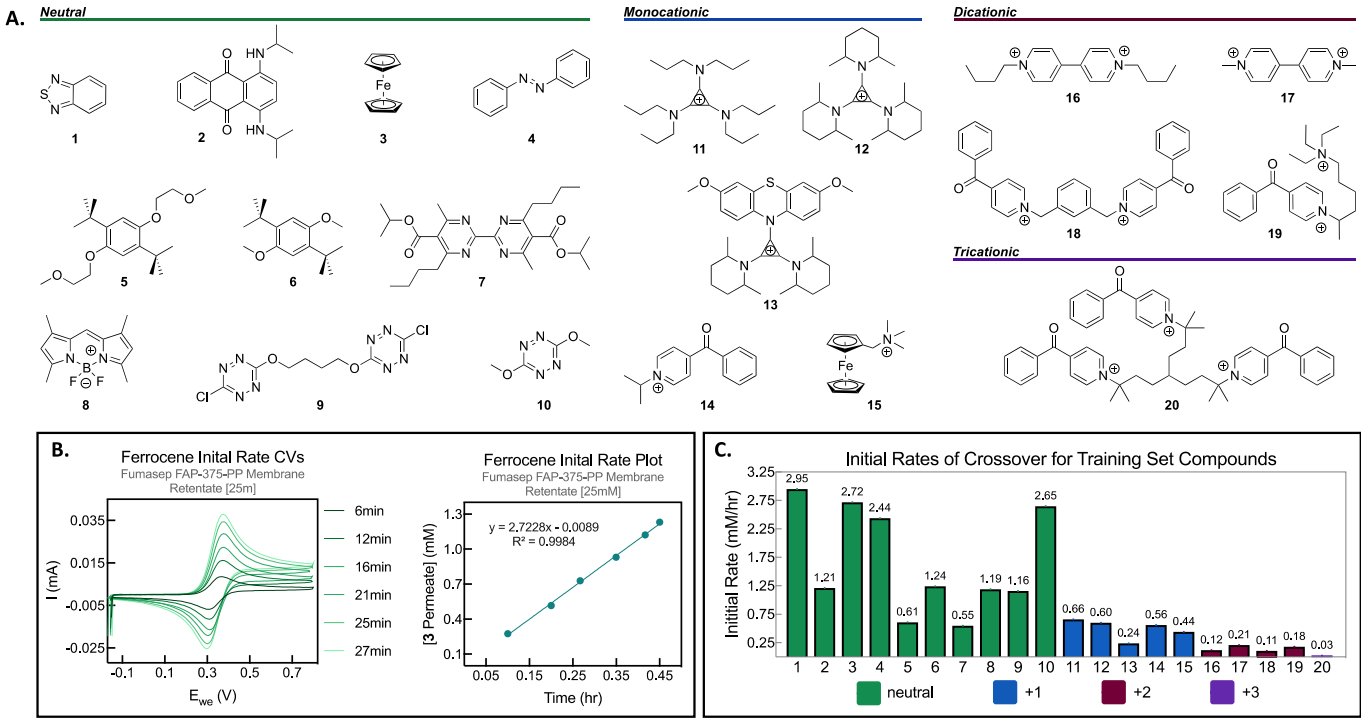

Figure 1. Diverse set of NARFB ROMs. **A.** Dataset used for model development. Anions omitted for simplicity (each charged compound is a PF6– salt. **B.** Representative cyclic voltammograms (CVs, left) of retentate as a function of time and initial rates plot (right). **C.** Initial rates for ROMs in Fig. 1A, grouped by charge.

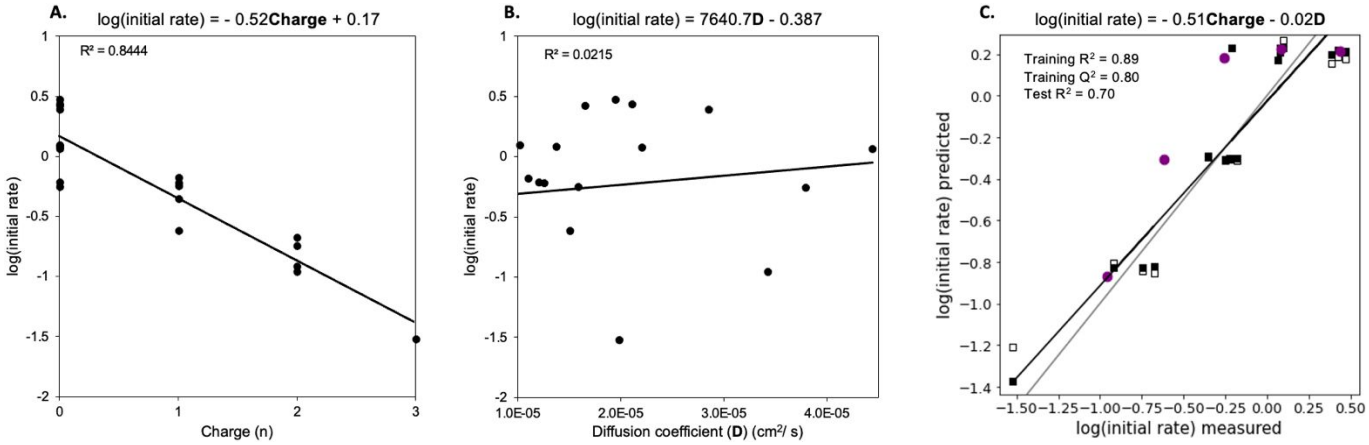

Figure 2. **A.** Univariate correlation between charge (n) and the log of initial rate of crossover. **B.** Plot of initial rate versus diffusion coefficient, showing no univariate correlation. **C.** Multivariate linear regression model containing charge (n) and diffusion coefficient (D) as descriptors.

We first examined the relationship between the crossover rate and the overall charge of the molecule (n). As shown in Figure 2A, a reasonable correlation is observed (R^2 = 0.84), as is expected for an AEM. This shows the anticipated trend that neutral ROMs cross over ~5-fold faster than monocations, which cross over ~5-fold faster than dications. However, within each integer charge state, there is significant variation (e.g., up to a factor of ~5 within the neutral molecules) that is not accounted for in this univariate correlation. This indicates that charge alone is insufficient to predict ROM crossover in this system. In an initial attempt to address this, we experimentally determined solution diffusion coefficients (D, often considered a proxy for the size of a molecule in solution)[24,52,53] for **1-20** using cyclic voltammetry.[54] Surprisingly, a plot of D versus crossover rate (Figure 2B) shows no correlation (R^2 = 0.02), indicating that this property has a minimal relationship with crossover rates under these conditions. Finally, we conducted linear regression of n and D with the crossover rates to assess whether a combination of these two descriptors could effectively model this system. As shown in Figure 2C, the model does not correlate better than charge alone, and lacks the granularity needed for accurate prediction of molecules within charge classes. We can also confirm the reluctance of incorporation of D in this model by the small coefficient associated with D (0.02 vs 0.51 for charge, n). Overall, these initial results motivated further statistical modeling to identify better descriptors for crossover in these systems.

Statistical Modeling

We pursued statistical modeling techniques, an approach we have previously used to design NARFB anolytes and catholytes.[19,23,49,55] We noted that the density functional theory (DFT)-based profiling approach that we typically use for quantitative analyses is not readily amenable to this diverse set of structures, since they lack a common structural core.[56] Therefore, we turned to quantitative structure-property relationship (QSPR)-type descriptors, which are better suited for global description of structurally diverse ROMs. The QSPR descriptors examined included charge, cLogP,[57] cLogS,[58] number of H-bond donors/acceptors, polar surface area, number of rotatable bonds, number of aromatic rings, number of amines and oxygens, globularity, and the van der Waals surface area and volume. We also reasoned that solution conformation was likely to impact crossover, so three-dimensional unrestrained conformational ensembles of each molecule were collected to describe the dynamic shape of each compound in solution. Quantitative descriptors describing

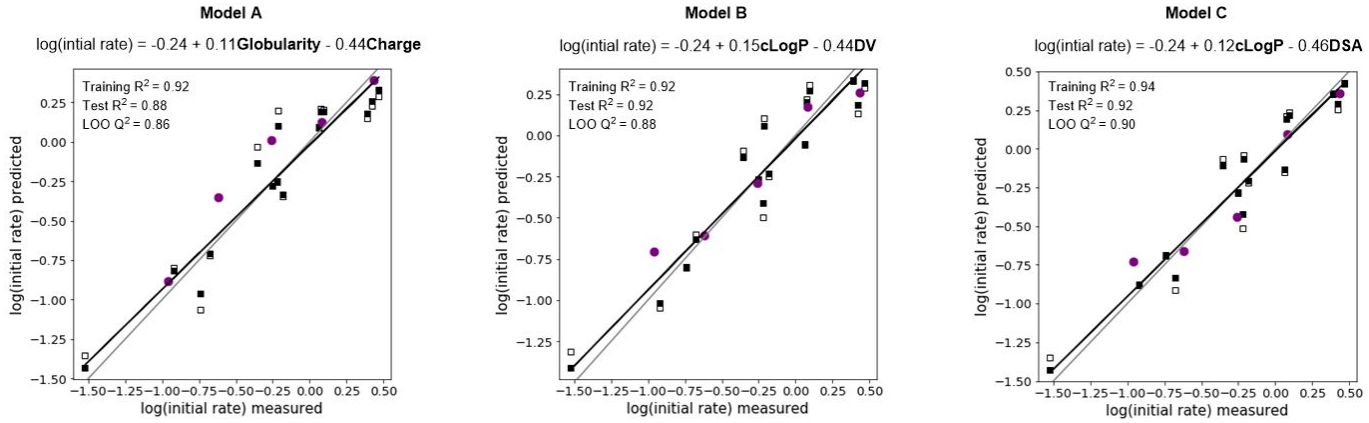

Figure 3. **A**. Linear regression Model A indicates one term that relates to increased rate (globularity) and one term that relates to decreased rate (charge). **B**. Linear regression Model B indicates one term that relates to increased rate (cLogP) and one term that relates to decreased rate (DV). **C**. Linear regression Model C indicates one term that relates to increased rate (cLogP) and one term that relates to decreased rate (DSA).

these ensembles, dynamic surface area (DSA) and dynamic volume (DV), were then computed. A full list of descriptors explored in this study can be found in the Supporting Information. This wide range of descriptors provides a set of parameters from which a forward-stepwise linear regression algorithm could determine the best-fit descriptors. Regression of this library of descriptors to the log of empirically determined initial rates enabled the construction of statistical models, which were evaluated by their statistical performance and interpretability.[56]

The best-fit models resulting from this process are shown in Figure 3. Model A is composed of two terms: globularity and charge. This model presents robust values for statistical evaluation (where the training R^2 is high, and the test R^2 and leave-one-out cross-validation Q^2 agree with both the training and test R^2 values, Fig. 2). Globularity is a measure of how spherical a molecule is (details for this calculation are included in the SI), and the positive coefficient indicates that more spherical molecules crossover faster. We hypothesize that this is because substrates that adopt a more spherical conformation can better fit through the pores in this membrane. The negative coefficient of charge indicates that as the formal positive charge of the molecule increases, the rate of crossover decreases. Therefore, cations permeate the membrane more slowly than neutral molecules. It should also be noted that the coefficient of charge is nearly four times as large as globularity, indicating an increase in the charge value is about four times as influential as the same (scaled) increase in globularity.

Though globularity and charge together accurately describe the behavior of the training set, we wondered whether these data could also be described by a continuous variable to provide more detail within charge classes, and whether size of the molecule had a direct influence on crossover rates. Two additional well-performing models were found that address these questions. Models B and C (Figure 3) contain a cLogP term and DSA or DV term, respectively. These models also present robust statistical metrics. In both cases, the training R^2 is high, and the test R^2 and leave-one-out cross-validation Q^2 agree with both the training and test R^2 values. The positive coefficient of the cLogP [calculated partition coefficient between n-octanol and water ($\log(c_{octanol}/c_{water})$, a measure of lipophilicity)] term in both models B and C indicates that ROMs that are more hydrophilic (as indicated by a small cLogP value, which, in the current series, tracks with molecules that have a larger overall positive charge), crossover more slowly. Because cLogP is a continuous variable, unlike charge, models B and C may be able to differentiate between molecules with the same overall charge. Model B also contains the DV term with a negative coefficient. DV is the volume of the conformational ensemble of a ROM (a readout of the effective size of a ROM in solution), and the negative coefficient indicates that as the DV increases, the rate of crossover decreases. Likewise, the negative coefficient of the DSA term (the surface area of a ROM's conformational ensemble) in model C indicates that as the DSA increases, the rate of crossover decreases.

Models A-C all effectively quantitatively describe the observed initial rates for this set of ROMs using interpretable terms. We next aimed to use the interpretation of the statistical models to design a moiety that could be tethered to an existing ROM and decrease its rate of crossover.

Implementation

We designed and synthesized a small set of ROMs (**21-26**; Table 1) based on the descriptors in models A-C. The goals of these studies were (1) to test how well these three models perform in predicting crossover for new molecules and (2) to identify tether groups that most effectively impede the crossover of neutral monomeric ROM cores. We selected dialkoxytetrazine as the core for derivatization for two reasons. First, the parent ROM, **10**, undergoes fast crossover (2.65 mM/h), so tether groups were expected to have a significant impact in this system. Second, these groups can be installed in 1-3 simple synthetic steps starting from commercial dichlorotetrazine. In all cases, the tether groups contain cationic tetraalkylammonium substituents, which are designed to increase the overall charge and to decrease the cLogP of the ROM. These were attached by linear alkyl chains of different lengths to minimize the spherical nature (globularity) and increase the effective size of the ROM (DSA, DV). Various substituents (methyl, benzyl, substituted benzyl) were incorporated on the ammonium nitrogen to assess the impact of size, symmetry, and hydrophilicity on crossover. Initial rates of crossover were determined for **21-26** using the same procedure as above, and the data are shown in Table 1.

All of the cationic tether groups slowed crossover by factors ranging from 5.4-fold to 43-fold compared to the first-generation molecule **10**. The incorporation of a single relatively

Table 1. Synthesis of Tethered ROMs to Decrease Rate of Crossover[a]

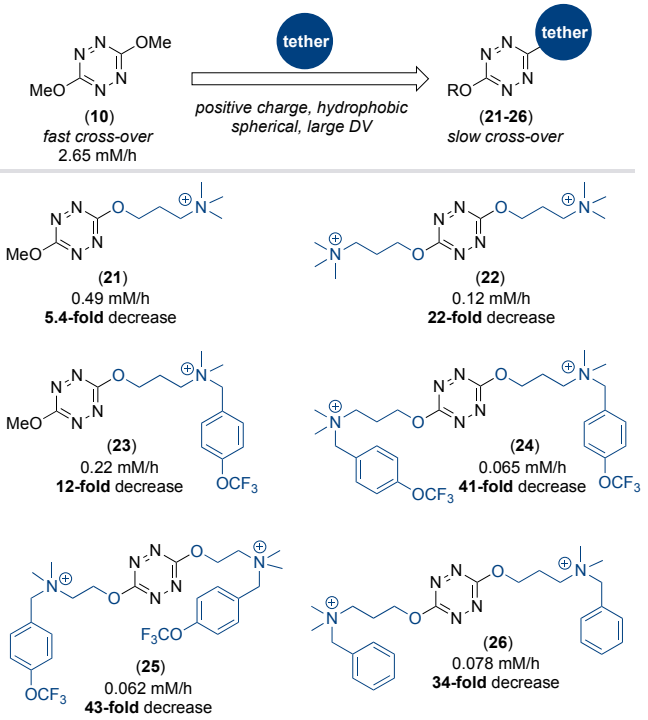

[a]Anions omitted for clarity. All compounds are PF_6 salts

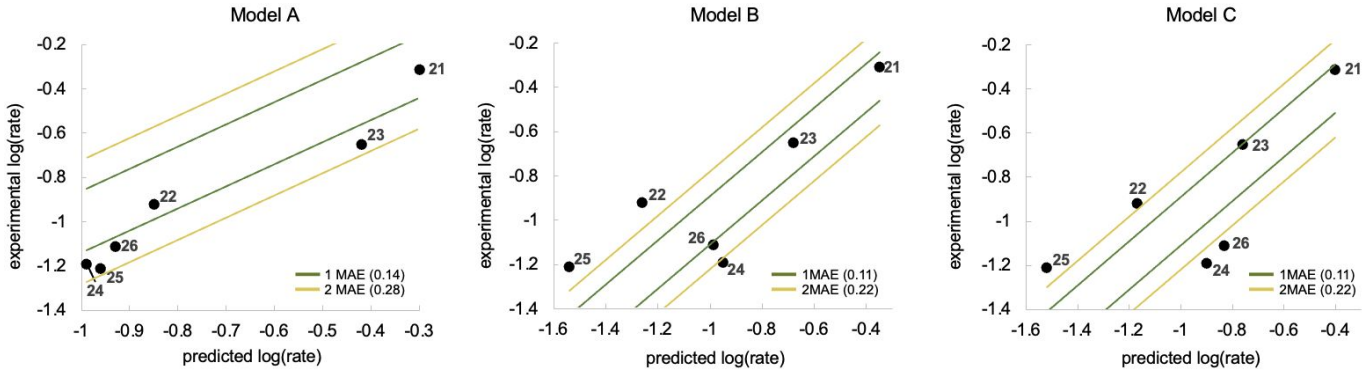

Figure 4. Predicted log(rate) of crossover versus actual log(rate) of crossover for tethered ROMs. Model A predicts 33% of data within 1MAE and 100% of data within 2MAE. Model B predicts 33% of data within 1MAE and 50% of data within 2MAE. Model C predicts 33% of data within 1MAE and 33% of data within 2MAE.

small and spherical trimethylalkylammonium tether group (**21**) resulted in a 5.4-fold decrease in the initial rate of crossover, while introducing two of this group (**22**) led to a 22-fold decrease. Increasing the size and decreasing the globularity of the tether by replacing a methyl with a *para*-trifluoromethyoxybenzyl led to larger 12- and 41-fold decreases for the mono- (**23**) and bis- (**24**) tether compounds, respectively. In contrast, minimal difference in crossover was observed upon shortening the chain by one carbon (compare **24** to **25**) or removing the OCF_3 group (compare **24** to **26**). To quantitatively assess models A-C, we compared the predicted crossover rate by each of the three models to the experimental data for **21-26** (Figure 4). All three models capture the magnitude of rate decrease in their predictions. Model A successfully predicts the quantitative rate of crossover for 33% of the tether molecules within 1 mean absolute error (MAE). Within 2 MAE, model A predicts 100% of the quantitative rate data. Models B and C only predicted 50% and 33% within 2 MAE, respectively. Overall, model A is the most accurate at predicting the quantitative rate of crossover for novel ROMs, however, models B and C still give insight to how to interpret the relative rate of crossover between compounds.

Conclusions

Overall, this study describes our development of several models for the crossover of structurally diverse redox active small molecules with the organic-solvent compatible AEM Fumasep FAP-375-PP in MeCN/KPF_6. As expected, the overall charge of the molecule plays an important role in crossover, with neutral > monocation > dication > trication. However, we show that charge alone is insufficient to fully predict crossover rates, as there is significant variation among ROMs with the same overall charge. We used QSPR analyses to identify globularity, dynamic volume, dynamic surface area, and clogP as useful descriptors leading to three statistically significant models for crossover. These models were then tested by evaluating various cationic tether groups for impeding the crossover of a dialkoxytetrazine-based ROM, resulting in derivatives with nearly 50-fold slower crossover rates. Overall, we anticipate that this approach will be more broadly applicable for evaluating and comparing cation exchange membranes as well as for identifying suitable ROMs for asymmetric non-aqueous redox flow batteries. Additionally, the incorporation of the tethers identified in Table 1 offers a synthetically straightforward approach for effectively deploying redox active small molecules in AEM-separated asymmetric flow batteries.

Conflicts of interest

There are no conflicts to declare.

Acknowledgements

This work was supported by the Joint Center for Energy Storage Research (JCESR), a U.S. DOE Energy Innovation Hub. M.S.S. and A.R.F. thank NIH grant R35 GM136271 for partial support in the context of developing molecular descriptors related to this work. Finally, we acknowledge Dr. Eugenio Alvarado for assistance with DOSY ^{1}H NMR diffusion coefficient measurements as well as Roy Wentz for providing custom electrodes for crossover experiments.

References

1. B. Dunn, H. Kamath, and J.-M. Tarascon, *Science*, 2011, **334**, 928-935.
2. G. L. Soloveichik, *Chem. Rev.*, 2015, **115**, 11533-11558.
3. E. Sanchez-Diez, E. Ventosa, M. Guarnieri, A. Trovo, C. Flox, R. Marcilla, F. Soavi, P. Mazur, E. Aranzabe, and R. Ferret, *J. Power Sources*, 2021, **481**, 228804.
4. K. Lourenssen, J. Williams, F. Ahmadpour, R. Clemmer, and S. Tasnim, *J. Energy Storage*, 2019, **25**, 100844.
5. Z. Huang, A. Mu, L. Wu, B. Yang, Y. Qian, and J. Wang, *ACS Sustainable Chem. Eng.*, 2022, **10**, 7786-7810.
6. R. Chen, *Curr. Opin. Electrochem.*, 2020, **21**, 40-45.
7. C. Zhang and X. Li, *Curr. Opin. Electrochem.*, 2021, **30**, 100836.
8. X. Wei, W. Pan, W. Duan, A. Hollas, Z. Yang, B. Li, Z. Nie, J. Liu, D. Reed, W. Wang, and V. Sprenkle, *ACS Energy Lett.*, 2017, **2,** 2187-2204.
9. J. Luo, B. Hu, M. Hu, Y. Zhao, and T. L. Liu, *ACS Energy Lett.*, 2019, **4**, 2220-2240.
10. J. Chai, A. Lashgari, and J. Jiang, ACS Symposium Series American Chemical Society, 2020, **1364**, 1-47.
11. L. Zhang, R. Feng, W. Wang, and G. Yu, *Nature Rev. Chem.*, 2022, **6**, 524-534.

12. F. Zhu, W. Gao, and Y. Fu, *Chem. Asian J.*, 2023, **18**, e202201098.
13. T. B. Schon, B. T. McAllister, P.-F. Li, and D. S. Seferos, *Chem. Soc. Rev.*, 2016, **45**, 6345-6404.
14. J. Noack, N. Roznyatovskaya, T. Herr, and P. Fischer, *Angew. Chem. Int. Ed.*, 2015, **54**, 9776–9809.
15. K. Gong, Q. Fang, S. Gu, S. F. Y. Lib, and Y. Yan, *Energy Environ. Sci.*, 2015, **8**, 3515-3530.
16. Y. Yan, P. Sitaula, S. A. Odom, and T. P. Vaid, ACS Appl. Mater. Interfaces, 2022, **14**, 49633−49640.
17. A. Shrestha, K. H. Hendriks, M. S. Sigman, S. D. Minteer, M. S. Sanford, *Chem.Eur.J.*, 2020, **26**, 5369 –5373.
18. P. Zuo, C. Ye, Z. Jiao, J. Luo, J. Fang, U. S. Schubert, N. B. McKeown, T. L. Liu, Z. Yan, and T. Xu, *Nature*, 2023, **617**, 299–305.
19. Y. Yan, S. G. Robinson, M. S. Sigman, and M. S. Sanford, *J. Am. Chem. Soc.*, 2019, **141**, 15301−15306.
20. Y. Yan, T. P. Vaid, and M. S. Sanford, *J. Am. Chem. Soc.*, 2020, **142**, 17564−17571.
21. Y. Yan, D. B. Vogt, T. P. Vaid, M. S. Sigman, and M. S. Sanford, *Angew. Chem. Int. Ed.*, 2021, **60**, 27039–27045.
22. Y. Yan, R. Walser-Kuntz, and M. S. Sanford, *ACS Materials Lett.*, 2022, **4**, 733−739.
23. Y. Yan, L. Zhang, R. Walser-Kuntz, D. B. Vogt, M. S. Sigman, G. Yu, and M. S. Sanford, *Chem. Mater.*, 2022, **34**, 10594−10605.
24. S. E. Doris, A. L. Ward, A. Baskin, P. D. Frischmann, N. Gavvalapalli, E. Chénard, C. S. Sevov, D. Prendergast, J. S. Moore, and B. A. Helms, *Angew. Chem. Int. Ed.*, 2017, **56**, 1595–1599.
25. M. Burgess, J. S. Moore, and J. Rodríguez-López, *Acc. Chem. Res.*, 2016, **49**, 2649−2657.
26. E. C. Montoto, G. Nagarjuna, J. S. Moore, and J. Rodríguez-López, *J. Electrochem. Soc.*, 2017, **164 (7)**, A1688-A1694.
27. E. C. Montoto, Y. Cao, K. Hernández-Burgos, C. S. Sevov, M. N. Braten, B. A. Helms, J. S. Moore, and J. Rodríguez-López, *Macromolecules*, 2018, **51**, 3539−3546.
28. G. Nagarjuna, J. Hui, K. J. Cheng, T. Lichtenstein, M. Shen, J. S. Moore, and J. Rodríguez-López, *J. Am. Chem. Soc.*, 2014, **136**, 16309−16316.
29. K. H. Hendriks, S. G. Robinson, M. N. Braten, C. S. Sevov, Brett A. Helms, M. S. Sigman, S. D. Minteer, and M. S. Sanford, *ACS Cent. Sci.*, 2018, **4**, 189−196.
30. M. J. Baran, M. N. Braten, E. C. Montoto, Z. T. Gossage, L. Ma, E. Chénard, J. S. Moore, J. Rodríguez-López, and B. A. Helms, *Chem. Mater*., 2018, **30,** 3861−3866
31. Y. Yan, S. G. Robinson, T. P. Vaid, M. S. Sigman, and M. S. Sanford, *J. Am. Chem. Soc.*, 2021, **143**, 13450−13459.
32. D. Kim, M. S. Sanford, T. P. Vaid, and A. J. McNeil, *Chem. Eur. J.*, 2022, **28**, e202200149.
33. C. R. Peltier, Z. Rhodes, A. J. Macbeth, A. Milam, E. Carroll, G. W. Coates, and S. D. Minteer, *ACS Energy Lett.*, 2022, **7**, 4118−4128.
34. N. H. Attanayake, Z.Liang, Y. Wang, A. P. Kaur, S. R. Parkin, J. K. Mobley, R. H. Ewoldt, J. Landon, and S. A. Odom, *Mater. Adv.*, 2021, **2**, 1390-1401.
35. S.-J. Gong, D. Kim, E. Cho, S. S. Hwang, and J. Won, *Chemistry Select*, 2017, **2**, 1843–1849.
36. T. Xu, *Journal of Membrane Science*, 2005, **263**, 1–29.
37. S.-H. Shin, S.-H. Yun, and S.-H. Moon, *RSC Adv.*, 2013, **3**, 9095–9116.
38. T. Luoa, S. Abdua, and M. Wessling, *Journal of Membrane Science*, 2018, **555**, 429–454.
39. B. Hu, M. Hu, J. Luo, and T. L. Liu, *Adv. Energy Mater.*, 2022, **12**, 2102577.
40. I. Salmeron-Sanchez, J. Asenjo-Pascual, J.R. Avilés-Moreno, J.C. Perez-Flores, P. Mauleón, and P. Ocón, *Journal of Membrane Science*, 2022, **643**, 120020.
41. R. Chen, *ChemElectroChem*, 2019, **6**, 603–612.
42. Z. Wang, H. Wang, S. Qi, D. Wu, J. Huang, X. Li, C. Wang, J. Ma, *EcoMat.*, 2022; 4, e12200.
43. M. T. Ong, O. Verners, E. W. Draeger, A. C. T. van Duin, V. Lordi, and J. E. Pask, *J. Phys. Chem. B.*, 2015, **119**, 1535−154.
44. Fumasep FAP-375-PP is a fluorinated AEM that is polypropylene reinforced. It has a thickness of 70-80 μm, is effective in pH environments less than 4, is unstable at pH > 10, and has 2% dimensional swelling in 2 M H_2SO_4. Technical Data Sheet: Fumasep FAP-375-PP, https://www.fuelcellstore.com/spec-sheets/fumasep-fap-375-pp-technical-specifications.pdf, accessed August 10, 2023.
45. For a recent related study of cross-over of organic molecules as a function of molecular structure in aqueous flow batteries, see: T. Y. George, E. F. Kerr, N. O. Haya, A. M. Alfaraidi, R. G. Gordon, and M. J. Aziz, J. Electrochem. Soc. 2023, **170**, 040509.
46. M. Saito, Y. Kawamata, M. Meanwell, R. Navratil, D. Chiodi, E. Carlson, P. Hu, L. Chen, S. Udyavara, C. Kingston, M. Tanwar, S. Tyagi, B. P. McKillican, M. G. Gichinga, M. A. Schmidt, M. D. Eastgate, M. Lamberto, C. He, T. Tang, C. A. Malapit, M. S. Sigman, S. D. Minteer, M. Neurock, and P. S. Baran, *J. Am. Chem. Soc.*, 2021, **143**, 7859−7867.
47. J. J. Dotson, E. V. Anslyn, and M. S. Sigman, *J. Am. Chem. Soc.*, 2021, **143**, 19187−19198.
48. H. Moriwaki, Y.-S. Tian, N. Kawashita, and T. Takagi, *J Cheminform*, 2018, **10**, 4.
49. S. G. Robinson, Y. Yan, K. H. Hendriks, M. S. Sanford, and M. S. Sigman, *J. Am. Chem. Soc.*, 2019, **141**, 10171−10176.
50. The initial rates data were obtained using constant volume, concentration, membrane thickness, and membrane area. Using these constants, each could be directly converted to a permeability value using the permeability equation. These data are tabulated on p. S52.
51. Cross-over was measured at a higher concentration (90 mM) for select molecules (**3**, **14**, and **17**). As anticipated, this resulted in a corresponding increase in the initial rate but no change in the permeability value for each. The data are provided on p. S54.
52. G. D. De La Garza, A. P. Kaur, I. A. Shkrob, L. A. Robertson, S. A. Odom, and A. J. McNeil, J. *Mater. Chem. A*, 2022, **10**, 18745–18752.
53. Macchioni, G. Ciancaleoni, C. Zuccaccia and D. Zuccaccia, *Chem. Soc. Rev.*, 2008, **37**, 479–489.
54. Use of CV to determine diffusion coefficients is standard practice in related cross-over studies [for examples, see: refs 27, 29, 33, and 45]. For comparison, we also measured diffusion coefficients for selected molecules (**2**, **14**, and **16**) using DOSY ^{1}H NMR spectroscopy, and these are reported on p. S51. In general, the values obtained by DOSY were 10-30% lower than those from CV measurements, but the relative differences between molecules remain similar.

55. J. D. Griffin, A. R. Pancoast, and M. S. Sigman, *J. Am. Chem. Soc.*, 2021, **143**, 992−1004.
56. C. B. Santiago, J.-Y. Guo, and M. S. Sigman, *Chem. Sci.*, 2018, **9**, 2398–2412.
57. clogP values were calculated according to the following: [https://openmolecules.org/propertyexplorer/clogp.html, (accessed August 2023)].
58. cLogS is the calculated aqueous solubility of a compound. These values were calculated as follows: [https://openmolecules.org/propertyexplorer/aqueous-solubility.html, (accessed August 2023)].